Laser Repair and Clean of Extreme Ultraviolet Lithography Photomasks

Tod Robinson*[a], Jeff LeClaire[a], Iacopo Mochi[b], Ricarda Maria Nebling[b], Yasin Ekinci[b], Dimitrios Kazazis[b]

[a]Bruker BNSM RMRBU (United States), 430 S. Congress Ave., Ste. 7, Delray Beach, FL, USA 33445; [b]Paul Scherrer Institute (Switzerland) ODRA/119, Forschungsstrasse 111, 5232 Villigen PSI, Schweiz

ABSTRACT

This publication is a continuation of a prior work on the process space available for the repair and localized cleaning of extreme ultraviolet lithography (EUVL) photomasks with the fpIII femto-pulsed deep ultraviolet (UV) repair tool. This next phase of work was done in partnership with the Paul Scherrer Institute (PSI) to provide a more systematic examination of the process space. In these tests, specialized cells were produced to systematically test the effect of variations in the fpIII laser parameters with both carbon and HSQ (hydrogen silsesquioxane) absorber material pin dots on multilayer fields, according to design of experiments (DOE) methodology. Blank (no pin dot) test cells and pin dots were inspected both with nmVI AFM and PSI RESCAN EUV-actinic lensless metrology before and after laser processing. This data was then analyzed with full-factorial DOE, and less structured techniques, to provide insights into the capability of a modelled optimal fpIII laser process.

Keywords: Photomask, repair, clean, contamination, particle, laser, EUV, sub-resolution.

1. INTRODUCTION

1.1 Background

In prior work, proof of concept was shown for the application of ultrashort (femtosecond) pulse DUV laser repair systems to the removal of small, high aspect, contaminates from EUV photomasks with no detectable impact on printability[1] . The capability of the laser system was shown on both multilayer and absorber for defects with a number of different compositions, including metal, silicon, carbon, and unknown material (see top panel of Figure 1).

The bottom panel of Figure 1 shows initial work to determine laser parameter thresholds for detectable (by EUV printability) multilayer damage. These parameter values and ranges were then compared to those used in the demonstration repairs (top panel of Figure 1) where there was a successful repair yield of 77% for a total of 73 defects.

The next phase of work was done in partnership with the Paul Scherrer Institute (PSI) to provide a more systematic examination of the process space available for the repair and localized cleaning of extreme ultraviolet lithography (EUVL) photomasks with the fp-III femto-pulsed deep ultraviolet (UV) repair tool. In these tests, specialized cells were produced to systematically test the effect of variations in the fp-III laser parameters with different absorber material pin dots on multilayer fields and were inspected both with Merlin AFM and PSI RESCAN EUV printability inspection.

*tod.robinson@bruker.com; phone 1 561 330-0411; fax 1 561 330-0896; bruker.com

Photomask Technology 2020, edited by Moshe E. Preil, Proc. of SPIE Vol. 11518, 1151809 · © 2020 SPIE · CCC code: 0277-786X/20/$21 · doi: 10.1117/12.2573084

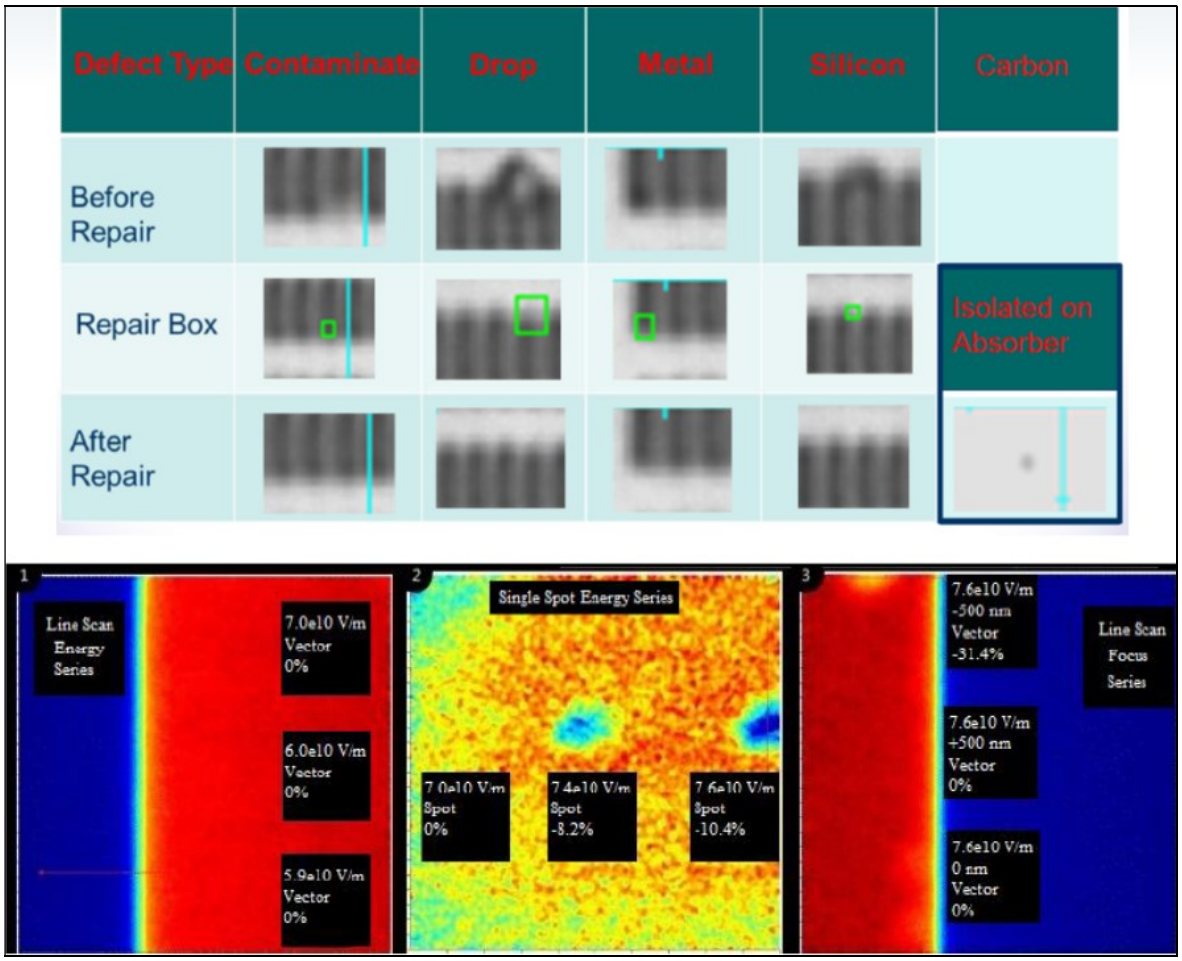

Figure 1. Prior proof of concept demonstration repairs of real particulate defects on an EUV photomask (top panel). Initial testing of laser parameter thresholds for printable multilayer damage (bottom panel).[1]

2. METHODOLOGY

2.1 Apparatus and overall test procedure

The apparatus for this work is summarized in Table 1. The first step of the overall process was to produce a test sample (and adaptor chucks to allow the sample to be loaded in mask repair toolsets) designed specifically for systematic laser repair process testing. A standard test sample was produced by PSI that consisted of repeating cells of different pin dot type absorber defects on multilayer (see Figure 3). This sample was then to be inspected with the RESCAN apparatus for EUV printability of the defects before laser repair and then shipped to Bruker RMR for AFM inspection before laser repair. After these AFM scans, laser repairs are performed on each of the pin dot defects in the targeted test die using varying laser parameters determined from pre-planned full factorial design of experiments. Once these test repairs are performed, the same sites were AFM scanned to determine the topographic changes (if any) of each of these defects. In the final stage, the sample was shipped back to PSI where it was once again inspected with the RESCAN apparatus for EUV printability. Other dies were also inspected for additional (originally unplanned) tests as well as to provide a supplement of pre repair defect data (there were indications in AFM scans that defect variations were similar for the same sub die location).

Table 1, summary of the apparatus used in this work

Purpose	Apparatus
Laser Photomask Repair	Bruker RMR fp-III
EUV Printablity Inspection	PSI RESCAN
AFM Inspection	Bruker RMR Merlin Nanomachining Tool

2.2 Apparatus review: RESCAN EUV metrology

RESCAN is a lensless microscope dedicated to EUV mask inspection operating at the Swiss Light Source synchrotron.[2] The microscope relies on coherent diffraction imaging (CDI) to reconstruct the complex amplitude of the mask surface. A coherent EUV beam is focused on the sample surface with an angle of incidence of 6 degrees. The sample plane is scanned, and a pixel detector records the diffracted light for each position of the object. The complex amplitude of the sample is reconstructed using ptychography[3], a noise-robust CDI technique that makes it possible to retrieve the phase and the amplitude of the object under investigation. RESCAN can detect amplitude defects as small as 50x50 nm^2 and characterize the phase of buried structures with an uncertainty of 2%.[4] In the current experiment, each of the reconstructed images has a pixel size of 32.5 nm and a spatial resolution of 45 nm. Each corresponding dataset is constituted by 141 diffraction patterns, covering a sample area of about 450 μm^2.

2.3 Apparatus review: fp-III Femtosecond Laser Photomask Repair System

The fp-III photomask repair tool employs a deep ultraviolet (DUV) 258 nm wavelength, femtosecond pulsed laser with high numerical aperture (NA) objectives. Compared to prior toolsets, the fp-III has increased stability, reliability, and a smaller cleanroom footprint. Repairs are performed with one of two different objective lenses. The 50X objective is most often used for through-pellicle repairs and dry cleaning (due to its longer working distance) and typically shows thin film removal beam burn diameter around 300 nm in diameter. The 150X, or highest magnification objective, is used when there is no pellicle mounted on the mask (this is automatically detected at mask load, and if a pellicle is present, this objective is locked out or disabled from being selected). The nominal beam burn diameter for the 150X on most photomask absorbers is approximately 200 nm. Another unique feature of the fp-III is that it has integrated features to support particle and surface clean processes that allow for EUV photomask defect selective repair and clean with potentially no detectable mask damage.

Figure 2, fp-III advanced laser photomask repair system

2.4 Sample for RESCAN EUV Metrology

Figure 3 shows a summary of the test defect matrix pattern for the sample specifically made for the RESCAN apparatus. The sample's substrate was a silicon wafer cut to 2 x 2 cm with a testing pattern in the center and two reference patterns in the upper corners. All repairs and AFM scans were performed on the center test pattern only which included a 4 x 4 array of die with identical patterns and defects. Each die (labelled 0-9 then A-F as shown in Figure 3) was then comprised of a 3 x 3 array of sub die (referred to by row and column number, for example row1 column 2, or R1C2). Each sub die was even further comprised of 3x3 um square cells, each of which could contain up to 50 defects. With this very large number of defect sites, most of the repairs were focused on one die (die B as seen in Figure 3), additional test repairs were performed in R1C3 sub die of die F as well as some pre repair referencing metrology performed in dies A and C.

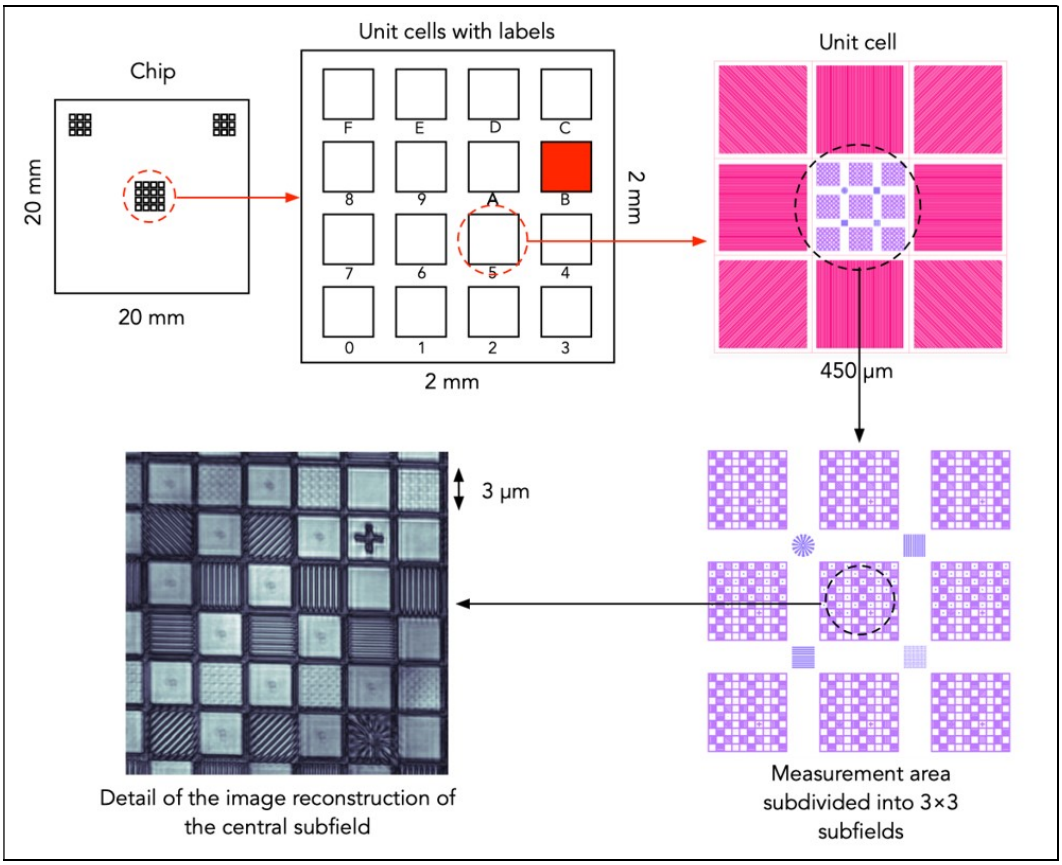

Figure 3, sample pattern layout for RESCAN EUV metrology

There were two different defect sizes (and aspects) evaluated and two different material compositions for the pin dots. These two materials were hydrogen silsesquioxane (HSQ) and carbon (C). The former material (HSQ) was the same material as the absorber material for all of the surrounding patterns and had a maximum height equal to the nominal absorber thickness of approximately 200 nm. These were high aspect pin dot defects found only in row 3 of the 3x3 sub die matrix shown in Figure 3. Although the HSQ defects were processed, it should be noted that results for HSQ and a third laser cleaning process are not included here, but will be reviewed in a future publication, and some promising results of a new process that provides an even more complete EUV repair and clean solution will be shown.

The other defect material, the carbon (C) pin dots, came in two different sizes and aspect ratios as shown in Figure 4. In the first row of the 3x3 sub die were the high aspect pin dot defects as shown in the left panel of Figure 4. As shown in the figure inset table, there were 91 of these C defects in die B with a z height range from 27.7 to 204.6 nm (mean 91.6) and a full-width half-max (FWHM) ranging from 131 to 306.5 nm (mean of 221.1). The low aspect c-pin dots in sub die row 2 had a z height range from 12.5 to 19.7 nm (mean 13.8) and a FWHM range of 499.5 to 682.5 nm (mean 578.6). Calculating the aspect ratios from these numbers (AR = z-height/FWHM) we get a range of 0.15 to 1.08 (mean 0.43) for the high aspect, and a range of 0.02 to 0.03 (mean 0.02) for the low aspect carbon pin dot defects.

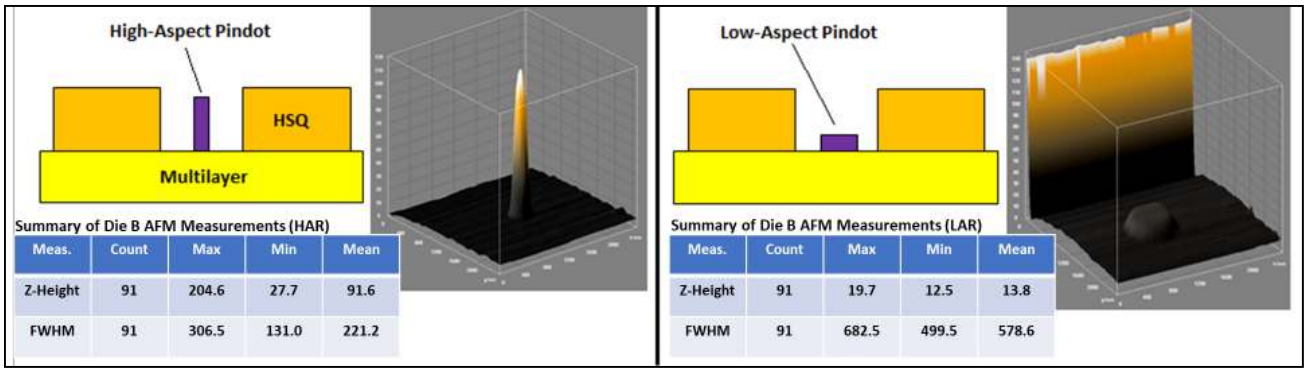

Figure 4. AFM inspection results for carbon pin dot defects in die B prior to laser test repairs. All units shown are in nanometers. A conceptual schematic, an example AFM scan, and raw AFM topographic measurements are shown for high aspect (left panel) and low aspect (right panel) defects.

In doing a large number of pre-repair AFM scans of die B, and other dies there were a couple of observations of interest that helped to define how the test procedure developed. The first observation was that although there was a large range in C defect sizes and aspect, there was some general groupings in the values. Thus, when the full factorial tests were defined for the laser processing parameters, the test sites were grouped so that their sizes were as close as possible to each other for that test. This meant that none of the tests were performed sequentially in placement on the sample but were scattered throughout the sub die row. It should be noted that for this work there are broad generalizations being made here in the defect sizes (high aspect versus low aspect defects). However, with further differentiation in these clusters, it may be possible to improve and clarify the analyses and modeling of the process data.

The second observation was that the variations in the high aspect carbon defects had a correlation to their location by, and within, each sub die. This feature of the test substrate was used to obtain comparable pre-data for those die where testing was performed, but no AFM pre-repair scans were collected.

Once the defect types were classified and grouped, the next consideration for test planning was the laser repair processes to be applied. Three different processes (parameters are not necessarily in order) with 2x different value ranges were evaluated. The first was the spot process where the laser beam is indexed to a location on the mask surface corresponding to the (DUV imaging) visual center of the defect. is the defect site is then exposed with a defined laser energy for some period of time and intensity. This process has three critical parameters for DOE tests (which for purposes here will be referred to as parameters A, B, and C). The second process is the area process where the beam is moved over the mask surface in a defined region according to a programmed series of movement vectors in the XY plane (of the mask surface). This process was tested with five defined critical processing parameters (parameters A through E). The final, and third, process was a new process still currently in development. A systematic DOE was not performed with this new process. Instead, a best of breed set of parameter values, determined from prior demonstration repairs were used. For the third process, the primary objective was to determine what the removal efficiency was for the high aspect carbon pin dot defects and whether there were any detectable effects on multilayer EUV printability.

In total, there were at least six different laser processing parameters which were targeted as being critical in DOE testing. These parameters included spot overlap, number of laser pulses exposed to the surface, motion vector speed, focus offset, vector spacing, and mean laser pulse energy.

3. RESULTS

3.1 High Aspect C-Defects (AFM) Repaired with Spot Process

Looking first at the results from testing the high-aspect carbon defects, one sees a representative example of the AFM result before (left side) and after (right side) laser test repair (using the spot process) in Figure 5. As seen in this case, there was a significant reduction in the maximum z-height of the defect (from 76 to 10 nm) and full width half max (FWHM, from approximately 206 to 74 nm) with less than 3 nm of topographically-resolved affect to the multilayer substrate. It should be noted that the overall slope seen in these scans are an artifact of thermal drift in the AFM scanning tool. This example shows what was observed over the hundreds of AFM scans manually examined; there was a clear variation in the amount of material removed according to the laser parameters applied in each test.

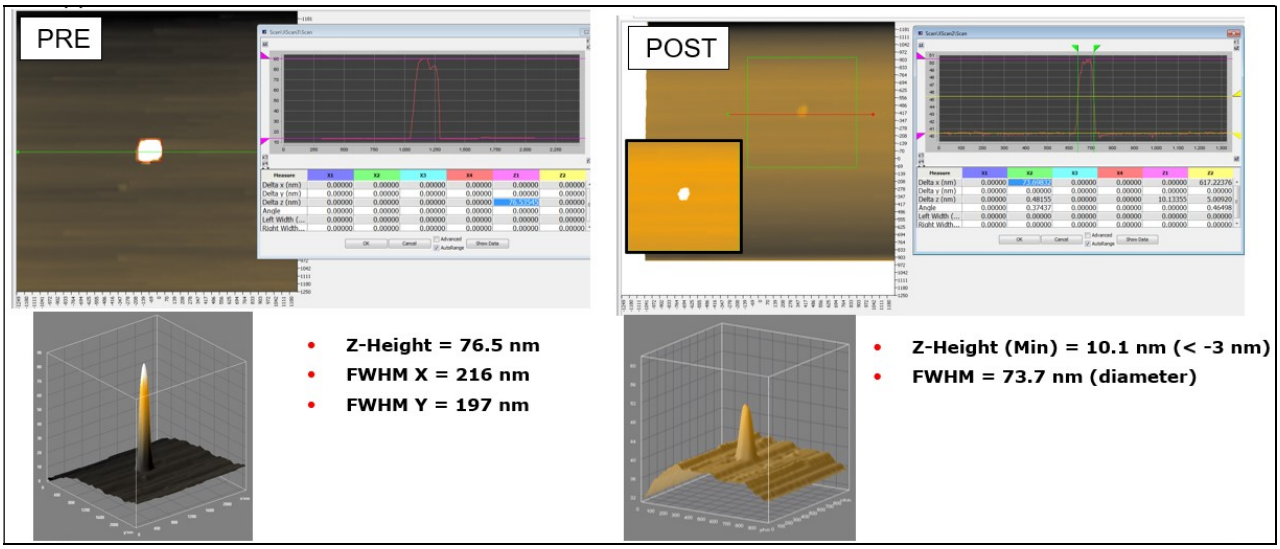

Figure 5. Typical AFM results for a high aspect (HAR) carbon pin dot defect pre (left side) and post (right side) laser test repair. In this example, there was a significant reduction in the maximum z-height (from 76.5 to 10.1 nm) and FWHM (from approximately 206 to 74 nm) with less than 3 nm topographic damage to the substrate. The overall slope to the surrounding surface seen here is an artifact of thermal drift in the AFM scanning tool.

Once the testing was performed, and all of the pre and post repair data was collected, it was first critical to determine what the best (or most physically representative) single measurement was to use in the DOE analysis. For the EUV imaging produced by RESCAN inspection, this step is trivial since the EUV amplitude attenuation (and later separate analysis, the relative phase shift) with respect to the surrounding references can be readily seen as the relevant measured response. With AFM topographic measures, however, the single best measure can be a little less clear. Figure 6 graphically reviews the raw measurements performed on the AFM scans. It also shows that all of the pin dot defects were generalized to be three dimensional Gaussian shapes. Maximum z-height, full width half max, and even the minimum height (to characterize any topographically measured affect to the multilayer Ru cap or multilayer) all characterize the defects size. However, all of these parameters can be correlated, possibly to variable degrees, in their impact on removal of the defect.

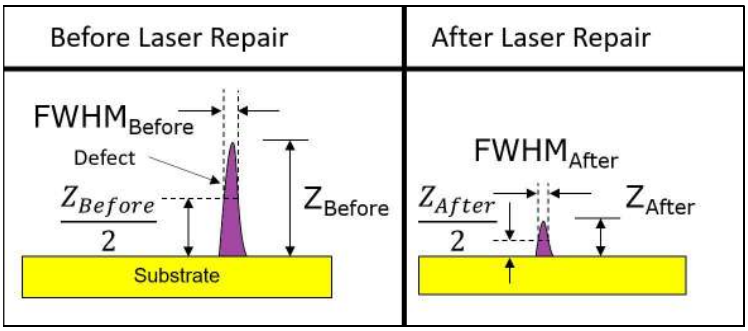

Figure 6. Schematic to define AFM measurement parameters on pin dot defects before (left panel) and after (right panel) laser repair processing.

Table 2 summarizes four different measures evaluated for use with the HAR carbon pin dots, and all of the other defects measured with AFM. These measures included z-difference, z-difference percent, volume difference, and volume difference percent. Refer to Table 2 for the equations used to calculate each of these measures. Full factorial DOE analyses were then separately run for each result and the consistency of the top three (highest impact) parameter across all of the HAR and LAR carbon pin dot tests for all interaction orders. As seen in the table, the volume difference percent had the most consistency across all of these tests. The volume difference percent can also be viewed conceptually as the best measure of defect removal, since it included both the z height and the FWHM and accounted for variations in both of these parameters for the defects before repair.

Table 2. Volume Difference Percent was best measure (in red box, applied to area DOE's).

Parameter Evaluation Matrix

Z-Difference

Test	1st Tier	2nd Tier	3rd Tier
HAR Test 1	C	AxBxC	AxB
HAR Test 2	AxB	BxC	A
LAR Test 1	AxB	B	C
LAR Test 2	A	AxC	B

Z-Difference Percent

Test	1st Tier	2nd Tier	3rd Tier
HAR Test 1	BxC	C	B
HAR Test 2	B	AxC	BxC
LAR Test 1	AxB	B	C
LAR Test 2	A	AxC	B

Volume Difference

Test	1st Tier	2nd Tier	3rd Tier
HAR Test 1	AxB	C	B
HAR Test 2	AxBxC	C	A
LAR Test 1	AxC	BxC	AxB
LAR Test 2	B	AxB	AxC

Volume Difference Percent

Test	1st Tier	2nd Tier	3rd Tier
HAR Test 1	AxC	AxBxC	C
HAR Test 2	AxC	C	BxC
LAR Test 1	AxC	AxB	BxC
LAR Test 2	B	AxB	AxC

Measurement Equations

$$\text{Z-Difference} = Z_{After} - Z_{Before}$$

$$Z - \text{Difference Percent} = \frac{(Z_{After} - Z_{Before})}{Z_{Before}}$$

$$\text{Volume} = 2\pi \cdot Z \cdot FWHM^2 \quad \textbf{(3D Gaussian)}$$

$$\text{Volume Difference} = \text{Volume}_{After} - \text{Volume}_{Before}$$

$$\text{Volume Difference Percent} = \frac{(\text{Volume}_{After} - \text{Volume}_{Before})}{\text{Volume}_{Before}}$$

3.2 Low Aspect C-Defects (AFM) Repaired with Spot Process

Figure 7 shows an example of the pre (left panel) and post (right panel) spot process repair AFMs of a low aspect carbon defect. Whereas the high-aspect defect removal primarily met expectations, the low aspect defect results were significantly more complex. As the aggressiveness of the laser removal process was increased, the main body of the defect remained, for the most part, unchanged. There was, however, the appearance of new peaks on top of the defects that often had the appearance of regularly spaced surface texturing. This texturing appeared to coincide with some combinations of parameter values while other defects were not visibly affected as seen in the AFM.

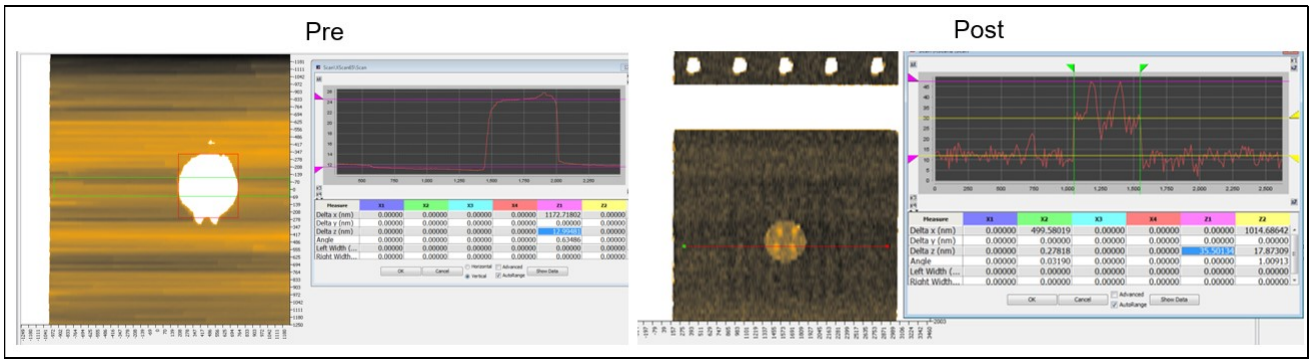

Figure 7. Low Aspect C-Defects (AFM) (right panel).

As seen in Figure 6, the AFM manual measurement methods developed for the high aspect, fairly 3D gaussian shaped, carbon defects would have difficulty measuring some of these textured post repair defects. The volume of these defects was approximated by using the peak height defined by the smaller peaks but adjusting the FWHM to accommodate for the reduced material volume.

3.3 Spot Process Analyses

The first stage in the overall spot process analysis was to apply full factorial design of experiments techniques to determine what were the pareto principle parameters for this process. The collected best metric (percent volume difference) data from all of the DOE's was applied to the full factorial design of experiments methodology as shown in Table 3. These results were then compared and contrasted for the two different parameter ranges (low range versus high range) for the two different defect size domains (high aspect versus low aspect).

For the high aspect carbon defects (AR~0.4), as seen in Table 3, parameters A and C appear to be the primary variables. At higher parameter A ranges, parameter C appears to become more dominant. Looking at the low aspect (AR~0.02) carbon defects in Table 3, the first order parameter interaction AxC appears to be the most important input at low ranges of parameter A. At higher ranges of A, parameter B becomes the more significant influence on the low aspect carbon defects.

These significant differences in the dominant input parameters suggests that one may be looking at four distinct processes in these four DOE tests. This further suggests that it may be required to separately model each of these regimes separately in their topographic changes with laser repair. This is unsurprising for the high versus low aspect carbon defects given the complexities in characterizing the post AFM scans of the latter.

Table 3. FFDOE Analyses of C pin dot AFM results.

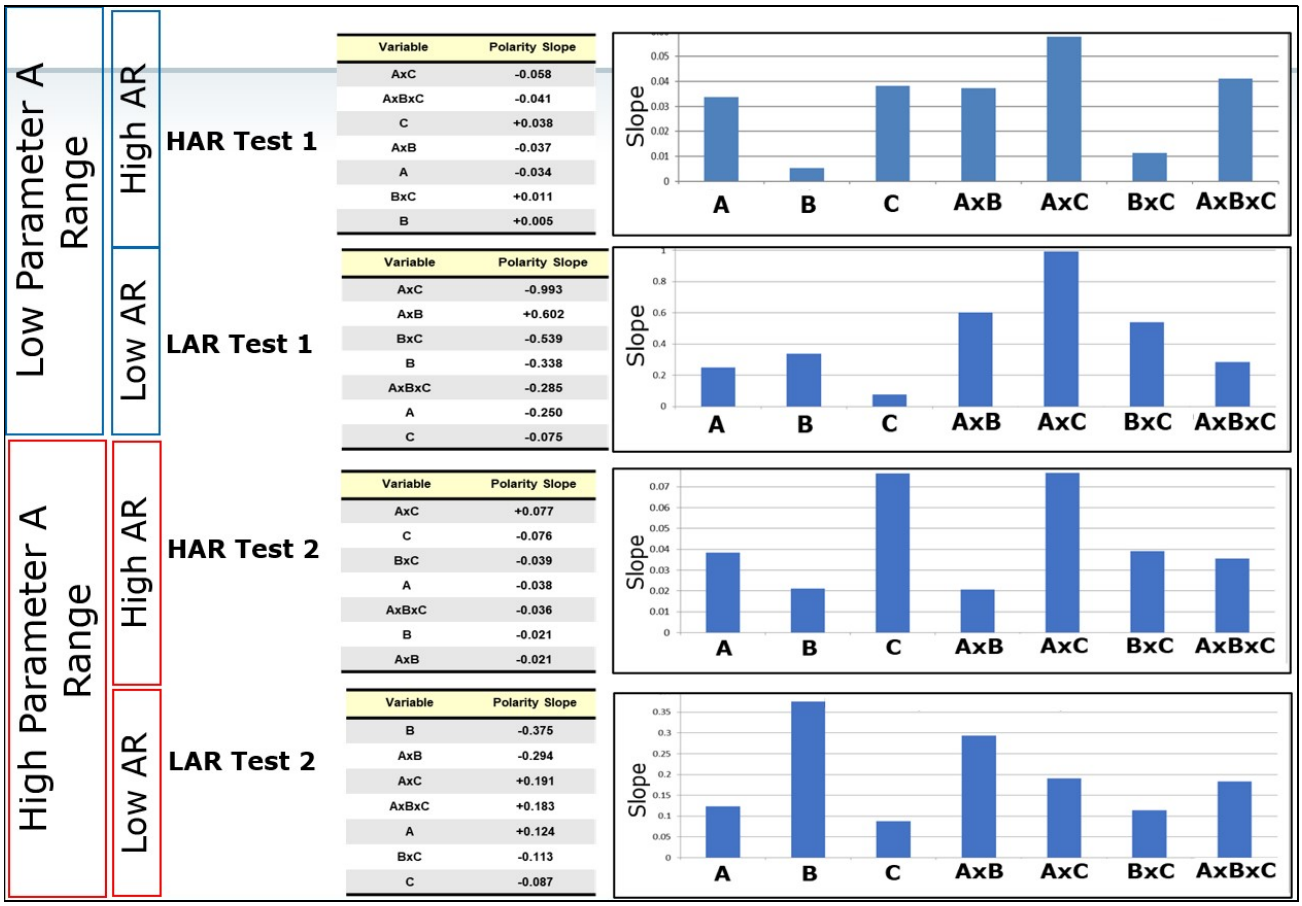

In analyzing the carbon pin dot defect data from spot process repairs with RESCAN EUV inspection, the amplitude attenuation results are the primary focus. Since the laser processes applied was intentionally highly variable, the defect that experienced the greatest change in reflectivity (referred to here as the best of breed repair) is of most interest. In this high aspect carbon defect repair, the actinic EUV relative reflectivity (referenced to untouched blank multilayer) went from 12% to 100%. Looking at the AFM results from this same repair, one sees that the maximum z-height went from 71 to 6 nm and the FWHM went from 234 to 148 nm with approximately 3.4 nm in Ru cap layer affect. For the rest of the test defect repairs, due to gaps in each of the full factorial DOE data sets in the EUV results, a FFDOE parameter response slope analysis was not possible. Instead, a search was performed for an analytical model to correlate to the data which was obtained (see Figure 8). As seen in Figure 8, which shows the current state of the empirically based analytical model search process, the high parameter range for both the high and low aspect carbon defects has a better correlation to the data. It is currently believed this is due to the lower signal to noise ratio for the lower input parameter ranges (Test 1). One curious observation is that both HAR and LAR models make significant use of the modulo ("mod"), and to a somewhat lesser degree, the logistic functions.

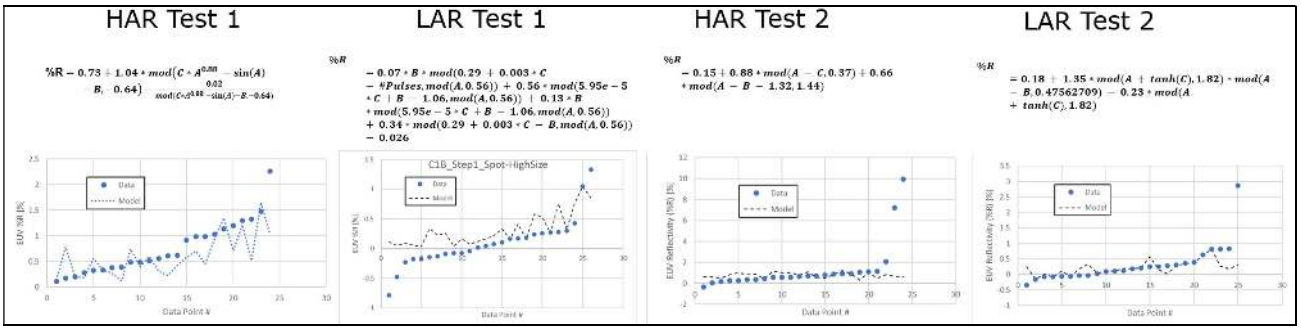

Figure 8. Analytical Empirical Fit Functions of C-Defects (RESCAN EUV) Repaired with Spot Process.

3.4 Area Process 2 (New Process)

Towards the end of the laser repair testing period, a novel process was used for proof of concept for (i.e. demonstration) contamination selective repairs. Initial results with this new process were obtained on DUV lithography optical masks, some examples of which are shown in Figure 9. As may be seen in this figure, this new area clean process was developed in response to the challenge of selectively removing very low aspect unknown (possibly organic or carbon-rich) contaminates that have become distributed over large areas (multiple microns in scale) across sensitive patterns on a DUV optical photomask. The existing area repair and clean process could potentially recover these areas. However, it would be very slow and arduous for the tool operator to accomplish this with possibly incomplete removal of the contaminates. Thus, a new approach was considered which would significantly speed up and simplify for complete removal of these contaminates.

Looking further at Figure 9, one may see that (as seen in the SEM as shown) the dark, spread out, contaminate regions appear to be completely removed. This was confirmed in DUV imaging on the laser tool both before and after processing. The only visible contaminates left after this treatment appear to be more discrete (possibly denser, possibly metallic or otherwise inorganic) nanoparticles which are typically easily and rapidly removed with the laser spot process on both absorber and substrate materials.

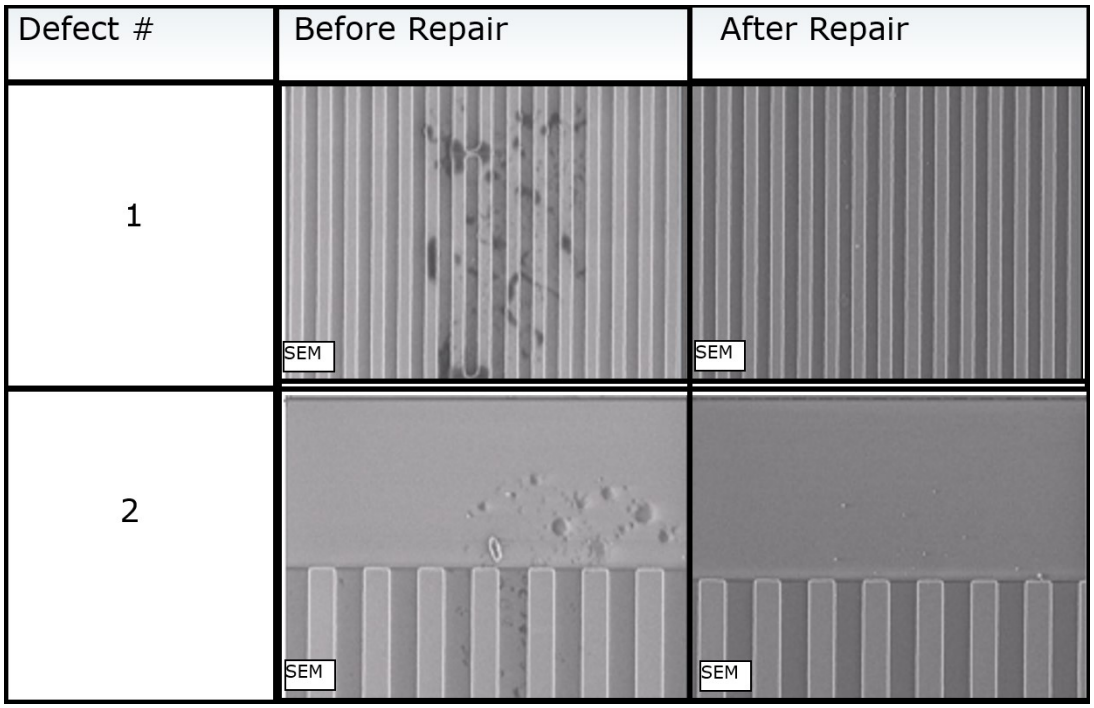

Figure 9. SEM proof of concept results for novel area clean repair process (area process 2) as performed on a DUV optical photomask. Large, low aspect (i.e. spread out) contamination.

Due to the dramatically successes in the proof of concept testing reviewed above with a DUV photomask, it was speculated that this same process could also be of significant utility to EUV photomask repair and clean. EUV masks can be easily contaminated with volatile organic compounds (VOC's) which can significantly absorb EUV wavelengths even when they are very thinly spread out over the surface. A test with this new area process was performed in sub die row 1, column 3 of die F as shown in Figure 10. This was not a pre-planned test so the subsequent AFM and RESCAN EUV results were compared to the same measurements in the same sub die in die A. As one may see in the left panel, these high aspect pure carbon pin dot defects were clearly visible in the fp-III laser repair tool's DUV imaging with both the 50X and 150X objectives prior to laser processing. This contrasted with the same imaging conditions of the same sub die after processing as is shown in the right panel. The pin dot defects in the centers of the test cells are no longer clearly discernable. This sub die was analyzed with AFM, and ultimately RESCAN EUV, post repair metrology.

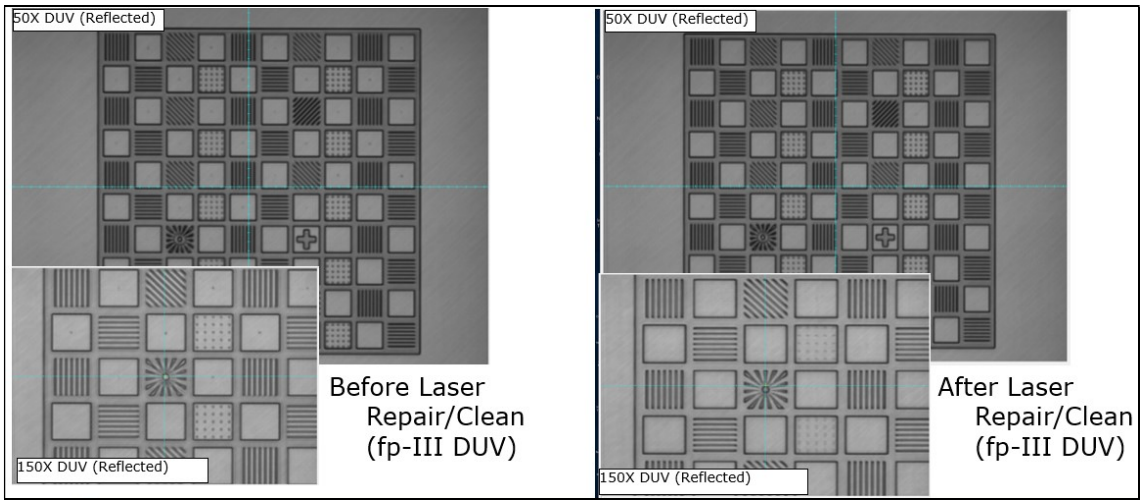

Figure 10. There was a significant reduction in the visibility of defects in DUV imaging (left panel before area process 2) after repair (right panel).

An example of one of these high aspect carbon pin dot defects after repair (in die F) with area process 2 in the middle panel of Figure 11 next to an AFM of a comparable reference from die A in the far left panel. In the far-right panel of this figure are the two histograms to compare the overall z height distributions between the repaired (in green) and unrepaired (violet) sub die. One may see in the comparison of these histograms that the mean, maximum, and minimum of the distribution were reduced by the area repair as well as the variance of the distribution. The difference is significant and clearly discerned. However, the reduction is qualitatively less than what was observed with the lower aspect contamination removed in the demonstration repairs in Figure 9.

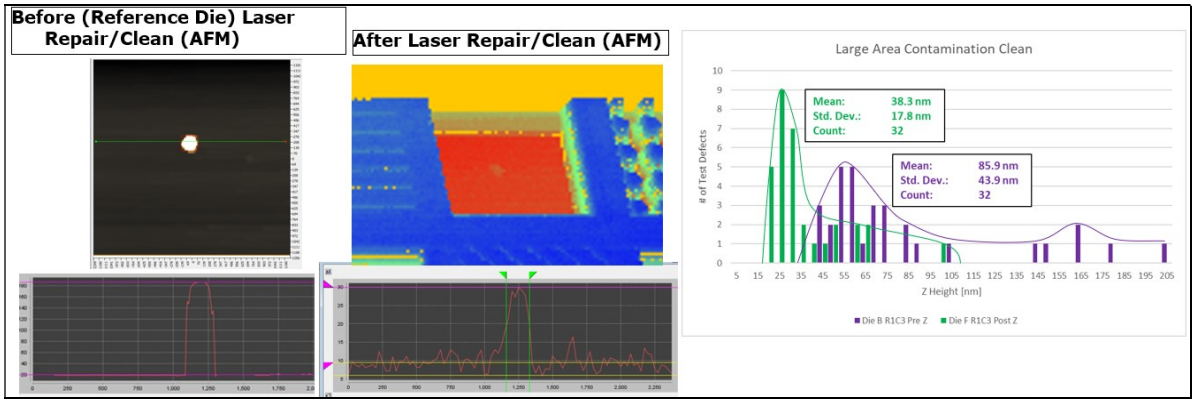

Figure 11. New Area, Low-Aspect Laser Clean Process. HAR C-Pin dots are significantly reduced, but not as much as with thinner, more spread out contaminates (Low AR or LAR).

Figure 12 shows a similar examination of the RESCAN EUV reconstructed inspection image data. In the far-left panel of Figure 12, the combined amplitude and phase shift image is shown for the reference sub die in die A. The middle panel is the comparable sub die after repair with area process 2. In these images to EUV actinic amplitude is denoted by the greyscale shading (with darker regions showing lower reflected amplitudes and thus more absorption) while the phase shift is shown by a shift in the RBG values relative to the surrounding reference areas. In the reference sub die image the high aspect carbon pin dots are visible as a region of darker greyscale shading in the center of the test. In the repaired sub die, these darker shading regions are no longer visible and there is no clear color shift, which indicates no

significant phase damage. Almost as important is that the repaired cells do not appear darker than the surrounding multilayer reference areas which indicates the selectivity of the high aspect defect reduction in actinic EUV printability.

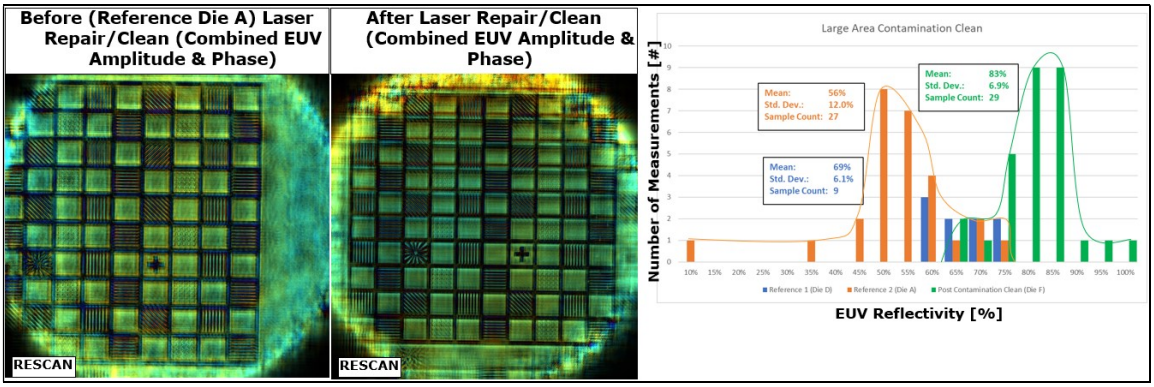

Figure 12. New Area, Low-Aspect Laser Clean EUV reflectivity (RESCAN). A pre repair reference sub die (in Die A) in row 1 column 3 (high aspect carbon defects) is shown in composite amplitude and phase shift RESCAN EUV reconstructed image (left panel). The same kind of result image is shown in the middle panel for the actual area process 2 test sub die (row 1, column 3 in die F). Each cell with a high aspect defect was

In the far-right panel of Figure 12, the histogram distributions for the relative amplitude (i.e. EUV reflectivity) are shown as it was for z-heights in Figure 11. As with the z-height histograms, the repaired defects (in green in the far-right panel of Figure 12) show discernable improvement than the unrepaired reference defects (in orange for die A and blue for die D). The repaired defects show increased EUV reflectivity in all of their statistics and a decreased variance in their distribution. It appears that the repair increased the mean reflectivity from 56 to 83% while reducing the standard deviation from 12 to 7%.

4. CONCLUSIONS

For carbon pin dot repairs using the established spot repair process, AFM pre and post laser repair data was analyzed in distinct regimes of defect aspect (high 0.4 AR, versus low 0.02 AR) and laser parameters (low and high ranges). No removal enhancement was observed for carbon defects of less than or equal to 0.02 AR in the range of laser parameter values generally safe for use on EUV photomasks. Parameter slopes clarified which laser parameters were most crucial to affecting pin dot defect percent volume change (AxC for high aspect and B for low aspect defects). This was confirmed in the prevalence of the parameters in the empirically based analytical models and modelling using neural networks (the latter not being shown in this work). These same empirically based analytical and neural network models with correlation to testing results were established for ongoing process for topological and EUV print optimization.

A novel area, laser-based process for low-aspect carbon/organics repair/clean was first introduced in demonstration repairs on a DUV optical photomask (Figure 9). The new process was successfully used in a complementary process ensemble with the spot process in this demonstration where the former removed low aspect (i.e. spread out) contaminates over large areas and the latter process was most effective with small particles. From the experience of this demonstration, it was believed this new process could be the final piece to complete the laser repair and cleaning solution for EUV photomasks, so it was initially tested on high aspect carbon pin dots on the sample to be sent to PSI for RESCAN EUV metrology. There was significant reduction in these defects seen in both AFM and RESCAN EUV amplitude although the degree of cleaning and removal was not as dramatic as was observed in the prior demonstration repairs of very low aspect contaminates. This reduction for possibly non-optimal defects, along with the lack of any detectable (non-selective) damage, reinforces the belief that this new low aspect and low density area process has the potential to be highly complimentary with the more established spot process which works best with dense (metallic), compact high-aspect nanoscale contaminates.

REFERENCES

[1] Tod Robinson, Jeff LeClaire, "Advanced laser repair of EUV photomasks," Proc. SPIE 11178, Photomask Japan 2019: XXVI Symposium on Photomask and Next-Generation Lithography Mask Technology, 111780K (27 June 2019); https://doi.org/10.1117/12.2534759.

[2] Iacopo Mochi & Yasin Ekinci (2019) Lensless EUV Lithography and Imaging, Synchrotron Radiation News, 32:4, 22-27, DOI: 10.1080/08940886.2019.1634433.

[3] Thibault P, Dierolf M, Bunk O, Menzel A, Pfeiffer F. Probe retrieval in ptychographic coherent diffractive imaging. Ultramicroscopy. 2009;109(4):338-343. doi:10.1016/j.ultramic.2008.12.011.

[4] Iacopo Mochi, Sara Fernandez, Ricarda Nebling, Uldis Locans, Rajendran Rajeev, Atoosa Dejkameh, Dimitrios Kazazis, Li-Ting Tseng, Serhiy Danylyuk, Larissa Juschkin, Yasin Ekinci, "Quantitative characterization of absorber and phase defects on EUV reticles using coherent diffraction imaging," J. Micro/Nanolith. MEMS MOEMS 19(1) 014002 (30 January 2020) https://doi.org/10.1117/1.JMM.19.1.014002.